Elucidation of the Effects of Bisphenol A and Structural Analogues on Germ and Steroidogenic Cells using Single Cell High-Content Imaging

Abishankari Rajkumar, Trang Luu, Marc A Beal, Tara S Barton-Maclaren, Bernard Robaire and Barbara F Hales

Supplementary Data Files

1. Supplementary Methods

Imaging Acquisition and Processing

Hoechst/Calcein/Lysotracker Red image processing

Image segmentation to distinguish between different cells was done using the Hoechst channel where cells were identified using their Hoechst stain (Method-B, Common threshold=0.2, Area > 30µM, Split factor=7, individual threshold=0.5, contrast>0.1). Once nuclei were selected, the Calcein stained cytoplasm was defined in segmented cells using the CalceinAM channel (Method A, individual threshold=0.1). Calcein mean signal intensity was determined using the Calculate Intensity Properties function following selected parameters (region of interest (ROI) population: nuclei, ROI region: cytoplasm). To exclude cells that were not unstained for Calcein the select population function was used (ROI population: nuclei selected, Method: Filter by property, Filter F1: Intensity Cytoplasm CalceinAM mean>1000). The numbers of lysosome spots stained with Lysotracker Red were determined from the nuclei selected population; the number of spots were located in segmented cells using the Lysotracker channel (ROI population=nuclei selected, ROI region=cell, Method A, relative spot intensity>0.075, splitting coefficient=1, calculate spot properties). The maximum intensity of lysosome staining was calculated using the Lysotracker Red Channel (ROI population: spots, ROI region: spot maximum), using exclusion criteria to remove outliers (ROI population: spots Method: Filter by property, Filter F1: Intensity spot maximum Lysotracker Red mean <20,000, Filter F2: spot area (px^2)<200). The output value for numbers of lysosome spots was divided by the numbers of nuclei to obtain the numbers of spots/cell.

Hoechst/MitoTracker Green/MitoTracker Red image processing

Image segmentation to distinguish between different cells was done using the Hoechst channel where cells were identified using their Hoechst stain (Method-B, Common threshold=0.4, Area > 30µM, Split factor=16.5, individual threshold=0.2, contrast>0.1; Hoechst Intensity- ROI population: nuclei, ROI region=nucleus, method- standard mean; Nuclei selected population- ROI population: nuclei, Method: Filter by property, Filter F1: intensity nucleus Hoechst <10,000 to remove outliers), Calculate Morphology Properties function (Nucleus Output= ROI population: nuclei, ROI region: nucleus, mean: standard-area roundness; Cell Output= ROI population: nuclei selected, ROI region: cell, method= standard- area roundness). Total mitochondrial intensity was determined by defining the image region (Channel: MitoTracker Green, ROI population: nuclei selected, ROI region: cell, Method: common threshold, threshold=0.35, split into objects, output population: Mitogreen, output region: mitochondria) followed by Calculate Intensity Properties function (Channel: MitoTracker Green, ROI population: Mitogreen, ROI region: mitochondria, Method-standard-mean). The intensity of active mitochondria was determined by Calculate Intensity Properties function (Channel: MitoTracker Red, ROI population: Mitogreen, ROI region: mitochondria, Method-standard-mean). Active mitochondria relative to total mitochondria were determined by dividing the MitoTracker Red Intensity with that for MitoTracker Green.

Hoechst/Nile Red/CellMask DeepRed image processing

Image segmentation to distinguish between different cells was done using the Hoechst channel where cells were identified using their Hoechst stain (Method-B, Common threshold=0.4, Area > 30µM, Split factor=16.5, individual threshold=0.2, contrast>0.1; Hoechst Intensity- ROI population: nuclei, ROI region=nucleus, method- standard mean; Nuclei selected population- ROI population: nuclei, Method: Filter by property, Filter F1: intensity nucleus

Hoechst <20,000 to remove outliers) and defining the cytoplasm (Channel: CellMask Deep, nuclei, Method A: individual threshold=0.05). Lipid droplets were detected using the Finding Spots function (Channel: Nile Red, ROI population: nuclei selected, ROI region: cell, Method A: relative spot intensity>0.08, splitting coefficient=1, calculate spot properties) and nuclei selection was used to determine total lipid droplet spot areas and numbers/cell.

Hoechst/CellRox/Calcein image processing

Image segmentation to distinguish between different cells was done using the Hoechst channel where cells were identified using their Hoechst stain (Method-B, Common threshold=0.2-0.4, Area > 30µM, Split factor=7, individual threshold=0.4, contrast>0.1; Hoechst Intensity- ROI population: nuclei, ROI region=nucleus, method- standard mean; Nuclei selected population- ROI population: nuclei, Method: Filter by property, Filter F1: intensity nucleus Hoechst <10,000 to remove outliers) and defining the cytoplasm (Channel: Calcein, ROI population: nuclei selected, Method A: individual threshold=0.15; Finding Surrounding Region for background: Channel: Calcein, ROI population: nuclei selected, ROI region: cell, Method A: individual threshold=0.15). Calculate Intensity Properties function was used to calculate both Cellrox intensity (Channel: CellRox, ROI population: nuclei selected, ROI region: cell) as well as background (Channel: CellRox, ROI population: nuclei selected, ROI region: background) to determine corrected values (Calculate Properties: ROI population: nuclei selected, Formula A-B, A=intensity of Cellrox, B=intensity background Cellrox).

Final readouts of all values from the Columbus processing and analyses system were mean values/well. Values were averaged between replicates to determine mean values/condition/experiment.

2. Supplementary data

Supplementary data Table 1: Live-cell dyes used during high-content imaging analyses.

Dye	Endpoint Assessed	Dilution	Source
CalceinAM	cell viability	1:1,000	Invitrogen
Hoechst 33342	nuclear morphology	1:2,000	Invitrogen
MitotrackerGreen FM	mitochondria quantification	1:2,000	Invitrogen
MitotrackerRedCMXRos	mitochondria activity	1:2,500	Invitrogen
LysotrackerDND99	lysosome quantification	1:6,666	Invitrogen
Nile red	lipid droplet quantification	1:100	Invitrogen
CellRox Deep Red	oxidative stress	1:2,500	Invitrogen
CellMask	plasma membrane	1:1,000	Invitrogen

Supplementary data Table 2: High-Throughput Toxicokinetics modeling parameters.

Acronym[1]	CASRN	Human.Clint	Human.Funbound.plasma	logP	MW	Css
BPA	80-05-7	28.61155556	0.0881	3.4237	228.28634	13.75
BPAF	1478-61-1	37.13131313	0.06454	4.5085	336.2291192	5.58
BPF	620-92-8	29.10169127	0.110349398	2.6886	200.2332	11.70
BPS	80-09-1	9.437737374	0.15853	3.0114	250.2704	126.54
BPM	13595-25-0	317.5133591	0.032901504	5.7496	346.462	4.27
BPTMC	129188-9-4	119.6474045	0.04336738	5.2301	310.4299	17.81

[1]BPA, BPAF, and BPS already had data available in HTTK and therefore, no input data was required.

Supplementary data Figure 1

Chemical concentrations at which no cytotoxicity was observed were used for the analyses of phenotypic endpoints using BMDExpress 2.2 (green boxes; grey boxes=significant cytotoxicity determined using Dunnett's test with Minitab19).

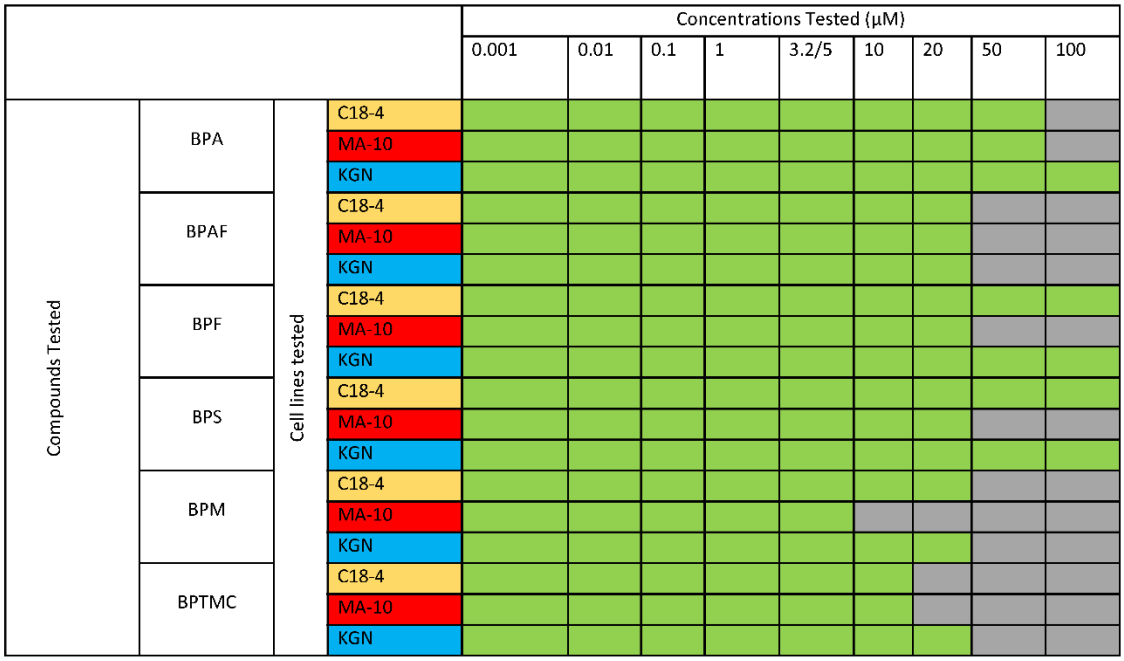

Supplementary data Figure 2

BMC models (significant-upregulated: yellow box, down-regulated: purple box; non-significant-grey) that were generated to observe the effects of bisphenols on various phenotypic endpoints.

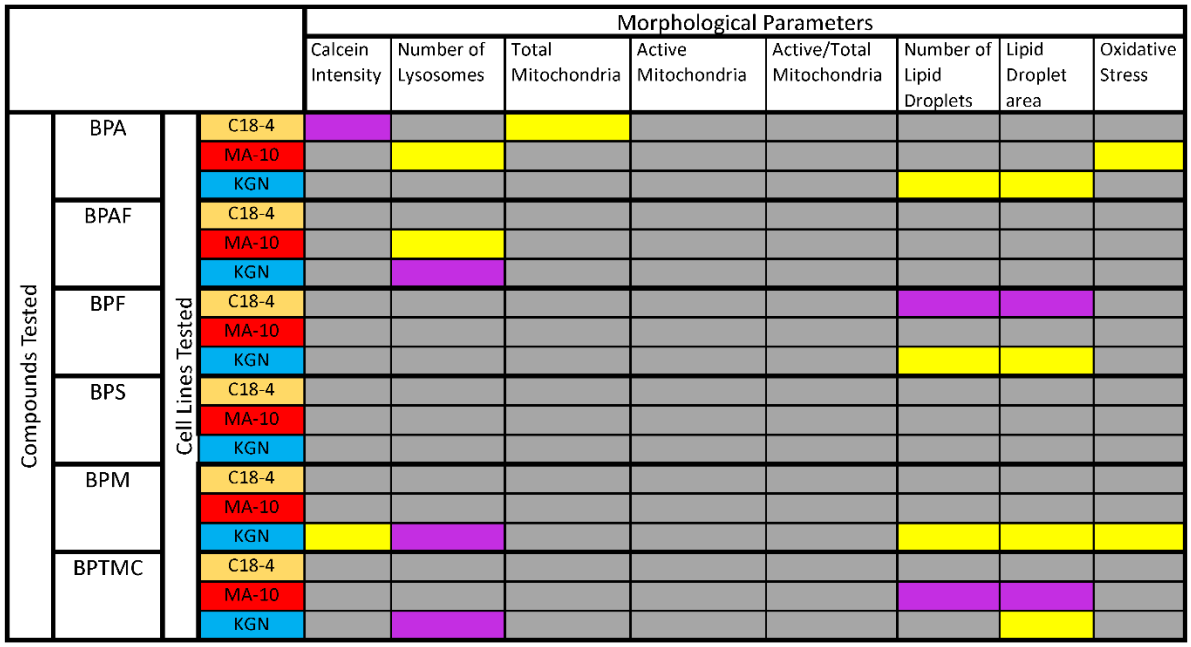

Supplementary data Figure 3

Comparison of bisphenol analog cell viability data from the literature (circles) with the BMC values reported here for C18-4, MA-10 and KGN cells (triangles). The y-axis depicts the lowest concentrations at which decreases were observed.

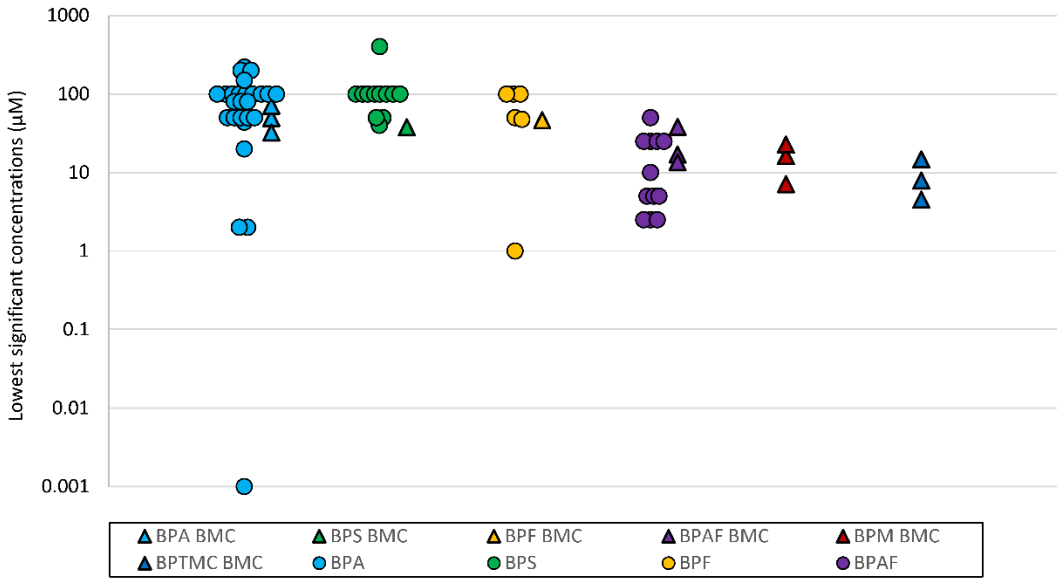

References for the data presented in Supplementary data Fig. 3:

Huang, M., Liu, S., Fu, L., Jiang, X. & Yang, M. (2020). Bisphenol A and its analogueues bisphenol S, bisphenol F and bisphenol AF induce oxidative stress and biomacromolecular damage in human granulosa KGN cells. *Chemosphere* **253**, 126707.

Jambor, T., Kovacikova, E., Greifova, H., Kovacik, A., Libova, L., Lukac, N. (2019). Assessment of the effective impact of bisphenols on mitochondrial activity and steroidogenesis in a dose-dependency in mice TM3 Leydig cells. *Physiol Res* **68**, 689–693.

Jiang, X., Yin, L., Zhang, N., Han, F., Liu, W. B., Zhang, X., Chen, H. Q., Cao, J., Liu, J. Y. (2018). Bisphenol A induced male germ cell apoptosis via IFNβ-XAF1-XIAP pathway in adult mice. *Toxicol. Appl. Pharmacol.* **355**, 247–256.

Kose, O., Rachidi, W., Beal, D., Erkekoglu, P., Fayyad-Kazan, H., Gumusel, B. K. (2020). The effects of different bisphenol derivatives on oxidative stress, DNA damage and DNA repair in RWPE-1 cells: A comparative study. *Journal of Applied Toxicology* **40**, 643–654.

Liang, S., Yin, L., Yu, K.S., Hofmann, M.C., Yu, X. (2017). High-content analysis provides mechanistic insights into the testicular toxicity of Bisphenol A and selected analogueues in mouse spermatogonial cells. *Toxicol. Sci.* **155**, 43–60.

Qi, S., Fu, W., Wang, C., Liu, C., Quan, C., Kourouma, A., Yan, M., Yu, T., Duan, P., Yang, K. (2014). BPA-induced apoptosis of rat Sertoli cells through Fas/FasL and JNKs/p38 MAPK pathways. *Reprod. Toxicol*. **50**, 108–116.

Qian, W., Zhu, J., Mao, C., Liu, J., Wang, Y., Wang, Q., Liu, Y., Gao, R., Xiao, H., Wang, J. (2014). Involvement of CaM-CaMKII-ERK in bisphenol A-induced Sertoli cell apoptosis. *Toxicology* **324**, 27-34.

Sidorkiewicz, I., Czerniecki, J., Jarząbek, K., Zbucka-Krętowska, M., Wołczyński, S. (2018). Cellular, transcriptomic and methylome effects of individual and combined exposure to BPA, BPF, BPS on mouse spermatocyte GC-2 cell line. *Toxicology and Applied Pharmacology* **359**, 1–11.

Téteau, O., Jaubert, M., Desmarchais, A., Papillier, P., Binet, A., Maillard, V., Elis, S. (2020). Bisphenol A and S impaired ovine granulosa cell steroidogenesis. *Reproduction* **159**, 571–583.

Wang, C., Fu, W., Quan, C., Yan, M., Liu, C., Qi, S., Yang, K. (2015). The role of Pten/Akt signaling pathway involved in BPA-induced apoptosis of rat sertoli cells. *Environmental toxicology* **30**, 793-802.

Xin, L., Lin, Y., Wang, A., Zhu, W., Liang, Y., Su, X., Hong, C., Wan, J., Wang, Y., Tian, H. (2015). Cytogenetic evaluation for the genotoxicity of bisphenol-A in Chinese hamster ovary cells. *Environmental toxicology and pharmacology* **40**, 524-529.

Yin, N., Liang, X., Liang, S., Liang, S., Yang, R., Hu, B., Cheng, Z., Liu, S., Dong, H., Liu, S., Faiola, F. (2019). Embryonic stem cell-and transcriptomics-based in vitro analyses reveal that bisphenols A, F and S have similar and very complex potential developmental toxicities. *Ecotoxicology and environmental safety* **176**, 330-338.

Zhu, X., Tian, G.G., Yu, B., Yang, Y., Wu, J. (2018). Effects of bisphenol A on ovarian follicular development and female germline stem cells. *Archives of toxicology* **92**, 1581-1591.